京都大学防災研究所年報 第 54 号 B 平成 23 年 6 月
Annuals of Disas. Prev. Res. Inst., Kyoto Univ., No. 54 B, 2011

Analysis of Bed Variation around Bandal-like Structures

Hajime NAKAGAWA, Hiroshi TERAGUCHI, Kenji KAWAIKE, Yasuyuki BABA and Hao ZHANG

Synopsis

The present investigation is focused on river bed variation caused by flow patterns around Bandal-like structure in channels. This type of structure have been used from the past in the Indian Sub-Continent to protect the river bank from erosion and to maintain the navigational conditions in alluvial rivers as the Jamuna river in Bangladesh. Few laboratory studies and field observations using Bandal-like structures was realized to verify the real applicability of them as an alternative structure over conventional river training structures as groins (impermeable and permeable ones). To clarify the effectiveness of Bandals in river morphology, detailed investigation about the complex flow structures and sediment transport mechanism influenced by Bandal-like structures was realized. Laboratory experiments were conducted in a straight flume with two structures positioned on one side of channel to the measurements of the velocity field and bed level near the structures under live-bed scour condition. A morphological model based on unstructured meshes was developed to simulate the flow patterns and bed variation around these structures. The experimental and numerical results of flow distributions and bed level variation around each type of structure were analyzed. The Bandal-like structure shows promising results as the reduction of local scour around them and deposition of sediment at downstream of Bandals in comparison with the conventional structures as groins.

Keywords: Bandal-like structure, live-bed scour, 3D model, non-submerged condition

1. Introduction

In river engineering works, hydraulic structures as groins are widely used for such purposes as river training, stream bank protection, and rectifying navigable rivers (Copeland, 1983; Carling et al., 1996; Shields et al., 2003). Nowadays, due to the increasing on demand of structures which provide the above functions and can be adaptive within local socio-economic condition and would be environmentally compatible solution as well (Shields et al., 2003) an alternative type of such structures called Bandal-like structure are investigated.

Bandals are one of the local structures developed in the Indian Sub-continent to improve or maintain the flows depth for navigation during low flow season. The main characteristics of Bandal-like structures are that they obstruct the high velocity flow near the water surface through the upper blocked portion (plate) conducting it to the main channel and allow the reduced velocity flow to pass near the riverbed (lower opened portion). This flow condition added to the fact that the transported sediment is composed by bed load and suspended load, which has higher concentration near the bed, contributes to increase the deposited sediment amount at downstream of Bandals near the riverbank in alluvial rivers. They usually are oriented at an angle with the main flow direction

(40°) and provide indirect protection by diverting potentially erosive currents away from the riverbank and by guiding the flow in a desired channel course. These are made of naturally available materials such as bamboo and wood pieces (**Fig.1**) that are regarded as inexpensive method over conventional structures as impermeable groins.

In the literature, the investigations related to groins (or spur-dikes) have been presented by many researchers as Garde et al. (1961), Gill (1972), Rajaratnam and Nwachukwu (1983), Kuhnle et al. (1999), Melville and Coleman (2000), Kothyari and Ranga Raju (2001), Uijttewaal (2005), and Dey and Barbhuiya (2006). However, the main focus of most of studies has been on impermeable groins and studies related to different types of structures as permeable groins are very few (Mioduszewski et al., 2003; Nasrollahi et al., 2008; Zhang and Nakagawa, 2009).

In the Bandal-like structures case, few laboratory experiments (Rahman et al., 2004, 2006) and field observations (Sharmin et al., 2007) appear to have been conducted to investigate the overall bed configuration, including the scoured area and the deposition of the sediment around the Bandals. Rahman et al. (2004) developed an analytical formula to predict the local scour around the structures including the degradation of the main channel. In this study, the basic features of Bandals in terms of flow and sediment control were clarified under clear-water scour condition. However, they pointed out the necessity of more investigations with different Bandal spacing, alignment to the main flow and experiments under live-bed scour condition.

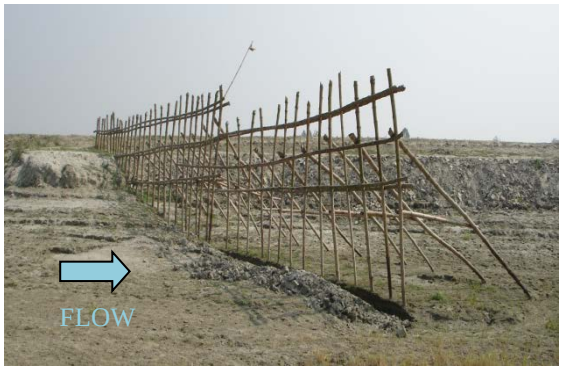

Fig.1 Bandal-like structures in Jamuna River (Pilot project, Bangladesh) – January 2010.

The flow field around a structure like Bandals is characterized by a complex 3D flow with the formation of downward flow and horseshoe vortex due to the effect of upper half plate at upstream and reduced velocity of flow passing through the structure at downstream (**Fig.2**). Moreover, the complexity of flow increases with the development of the scour hole.

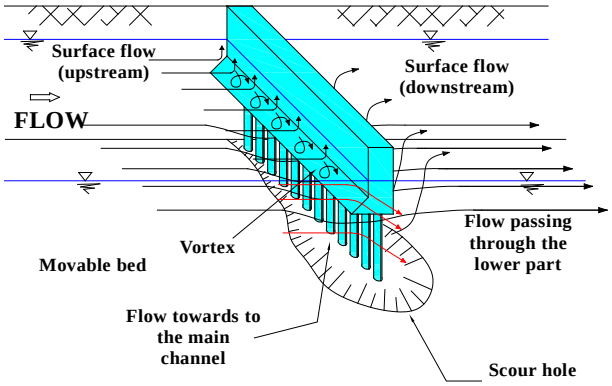

Fig.2 Flow structures around Bandal-likes structuture

To reproduce this kind of flow structures, numerical models have been widely applied to problems in hydraulic engineering. River modeling applications can be grouped into 1D, 2D and 3D models. 1D numerical model is very useful in practice, however its simulations results provide limited technical details. Though 2D models have been developed and used to solve the sediment problems in alluvial rivers. Whereas the area near the hydraulic structures has 3D effects on water flow and sediment motion, which are too complex for 2D models, 3D models for sediment transport in turbulent flows have become one of the most studied subjects in the field of river dynamics.

In comparison with 2D models, there are fewer applications of 3D models. Some recent works are: Wang and Adeff (1986) established a 3D mathematical model of river sediments by use of the finite element method; van Rijn (1987) using a combined mode, calculated the water flow by a 2D depth-averaged water model, and calculated the distribution of velocity along the water depth by a logarithmic velocity distribution equation, and further developed a combined 3D mathematical model; Shimizu et al. (1990) calculated water flows and bed deformation of meandering channels by using 3D sediment mathematical models; Wang and Jia (1995) developed a 3D sediment mathematical

model for simulating water flow, sediment motion and morphological change of alluvial rivers, especially local scour near a bridge pier; Wu et al. (2000) proposed a 3D mathematical model for total sediment based on Reynolds equations and k-ε turbulence model. Nagata et al. (2005) and Onda et al. (2007) developed a 3D numerical model using a non-linear k-ε model to predict the 3D flow patterns around hydraulics structures with reasonable accuracy in the simulation results.

In this study, the mechanism which affects the complex flow structures and bed variation around Bandal-like structures was investigated through the laboratory experiments and numerical model simulations. The experimental procedure was conducted in a straight flume with movable bed using two hydraulic structures (Bandal-like structure and groins) under non-submerged condition. The results from the experiments and numerical simulations were compared to verify the applicability of numerical model to reproduce the morphological changes around the Bandals. The information obtained from this analysis is very important for the correct design of Bandal-like structures in field applications (**Fig.3**).

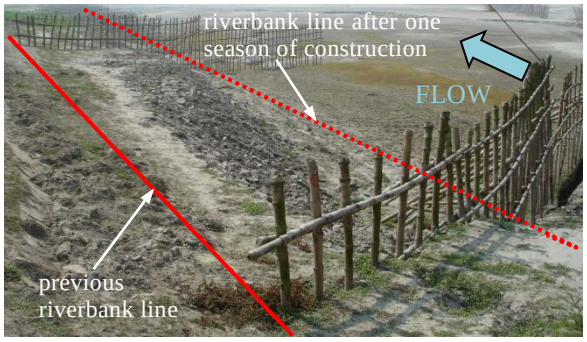

Fig.3 Application of Bandal-like structures on river bank protection in Jamuna river – Pilot project (January, 2010).

2. Numerical modeling

2.1. Hydrodynamic Model

1) Governing equations

The governing equations used in the numerical model are those of the 3D RANS (Reynolds-averaged Navier-Stokes) equations. The momentum and continuity equations expressed in a Cartesian coordinate system with the tensor notation read

$$\frac{\partial u_i}{\partial t}+u_j\frac{\partial u_i}{\partial u_j}=F_i-\frac{1}{\rho}\frac{\partial p}{\partial x_i}+\nu\frac{\partial^2 u_i}{\partial x_j\partial x_j}+\frac{1}{\rho}\frac{\partial \tau_{ij}}{\partial x_i} \quad (1)$$

$$\frac{\partial u_i}{\partial x_i}=0 \quad (2)$$

here u_i is the time-averaged velocity components (i=1, 2, 3); x_i is the Cartesian coordinate component; ρ is the density of the fluid; F_i is the body force; p is the time-averaged pressure; ν is the molecular kinematic viscosity of the fluid; $\tau_{ij}=-\rho\overline{u_i'u_j'}$ are the Reynolds stress tensors, and u_i' is the fluctuating velocity component. The k-ε model is used for the turbulence closure. The Reynolds tensors are acquired through the linear constitutive equation.

$$-\overline{u_i'u_j'}=2\nu_t S_{ij}-\frac{2}{3}k\delta_{ij} \quad (3)$$

where k is the turbulence kinetic energy; δ_{ij} is the Kronecker delta; ν_t is the eddy viscosity and S_{ij} is the strain-rate tensor and ε is the dissipation rate of the turbulence kinetic energy k. The model constants are used as suggested by Rodi (1980).

$$C_\mu=0.09, C_{1\varepsilon}=1.44, C_{2\varepsilon}=1.92, \sigma_k=1.0, \sigma_\varepsilon=1.3 \quad (4)$$

2) Numerical procedure

The present model uses a control volume-based method (Launder and Spalding, 1973; Patankar, 1980) to convert the differential conservation equations to algebraic equations that can be solved numerically. The method consists of integrating the differential equations about each control volume, yielding a finite volume equation that conserves each quantity on a control volume basis (Jameson et al., 1981). Collocated grid storage is used to define the discrete control volumes. To calculate the derivatives of the flow variables the power-law interpolation scheme is used (Patankar, 1980). The set of simultaneous algebraic equations is solved by a semi-implicit iterative scheme which starts from an arbitrary initial solution and converges to the correct solution doing several iterations. More detailed information about the numerical schemes, discretization methods, solution methods, equation solvers and the convergence criteria is given by Zhang et al. (2006).

3) Boundary conditions

Free surface: In the model, the water surface was considered as a rigid lid and defined as a plane of

symmetry. Symmetry implies that the normal velocity and the normal gradients of all variables are zero at the plane of symmetry.

Inlet: The definition of an inlet requires the values of the velocity vectors and turbulence properties. The inlet boundary is considered as a Dirichlet boundary and all the quantities are prescribed. In the pressure-correction equation, as the velocity field is given, the velocity correction is zero. And the Neumann boundary of zero gradients is used for the pressure.

Outlet: The outlet boundary has been set far from the structures area, a Neumann boundary with zero gradients is assumed here.

Impermeable wall: To estimate the effect of the wall on the turbulent flow, the wall function approach is adopted near impermeable boundaries, in which the piles (permeable groins) and Bandal-like structures (upper bended plate and lower permeable opening) is expressed with some fine meshes in the simulation.

4) Solution procedure

A usual procedure to judge solution convergence is to use a residual definition. The definition implies that convergence is reached when the normalized changes in variables between successive iterations are equal to or less than a certain limit. The algebraic equation systems are solved in an implicit decoupled way. Considering the sparseness and non-symmetry of the coefficient matrices, Krylov subspace iterative methods are preferred. The Bi-CGSTAB (Bi-Conjugate Gradient Stabilized) algorithm suggested by Sleijpen and Fokkema (1993) is employed in the model. For the pressure-velocity coupling the SIMPLE (Semi-Implicit Method for Pressure-Linked Equations) procedure was used. A comprehensive review of this algorithm is given by Versteeg and Malalasekera (1995).

The computational meshes used during the simulations are showed in **Fig.4**. To obtain a converged solution for 6 hours calculation on movable bed condition for each case, 2 weeks of computations were necessary on a powerful processor PC. In further study, an improvement using parallel computation, for example, should be implemented in the model to have reasonable results.

2.2 Sediment Transport Model

The sediment transport in open-channels is governed by the sediment mass-balance equation integrated over the water depth *h*, described below.

$$(1-\lambda)\frac{\partial z_b}{\partial t}+\frac{\partial(q_{Tx})}{\partial x}+\frac{\partial(q_{Ty})}{\partial y}+(E-D)=0 \qquad (5)$$

where z_b is the local bed level above datum; λ is the porosity of the bed material and q_{Tx}, q_{Ty} are the components of the total-load sediment transport in the x and y directions, respectively, E is the upward near-bed flux and D is the downward near-bed flux. For calculating the sediment transport rate, it is subdivided into bed load and suspended load.

1) Bed load transport

The bed load transport is calculated by using the Ashida-Michiue's empirical formula.

$$\frac{q_b}{\sqrt{(s-1)gd^3}}=17\tau_{*e}^{\frac{3}{2}}\left(1-\frac{u_{*c}}{u_*}\right)\left(1-\frac{\tau_{*c}}{\tau_*}\right) \qquad (6)$$

where q_b is the bed load; s is the specific gravity of sediment; d is the diameter of sediment; τ_*, τ_{*c}, τ_{*e} are the dimensionless shear stress, critical shear stress and effective shear stress, respectively; u_*, u_{*c} are friction velocity and critical friction velocity, respectively. In the Bandals simulations, the deformed bed from the experimental results was used as a fixed bed during the flow calculations.

2) Suspended load transport

For suspended load transport calculation, the convection-diffusion equation is used (van Rijn, 1987)

$$\frac{\partial c}{\partial t}+\frac{\partial}{\partial x_j}\left[\left(u_j-w_s\delta_{j3}\right)c\right]=\frac{\partial}{\partial x_j}\left(\frac{\nu_t}{\sigma_c}\frac{\partial c}{\partial x_j}\right) \qquad (7)$$

here c is the local sediment concentration, w_s is the sediment settling velocity, δ_{j3} is the Kronecker delta (j=3 indicating the vertical direction), σ_c is the turbulent Schmidt number relating the turbulent diffusivity of sediment to the eddy viscosity ν_t.

The near-bed fluxes appear as source terms and need to be evaluated. These are treated here as two separated processes; however in real conditions it is

generated by the simultaneous deposition and erosion process.

The deposition flux is calculated from

$$D = w_s C_a \tag{8}$$

where w_s is the sediment settling velocity and C_a is the ambient concentration near the bed. The near-bed equilibrium concentration at a reference level (C_a) is calculated by the deterministic expression of van Rijn (1987). For the erosion rate, it is generally assumed to be the one under equilibrium condition, which is

$$E = w_s C_e \tag{9}$$

here, C_e is the equilibrium concentration near the bed. The boundary conditions for the equation (7) are specified as follows. An equilibrium sediment concentration profile is given at the upstream inlet boundary. The concentration at the center of the cell closest to the bed (C) is computed from C_a with the aid of the Rouse (1937) equation.

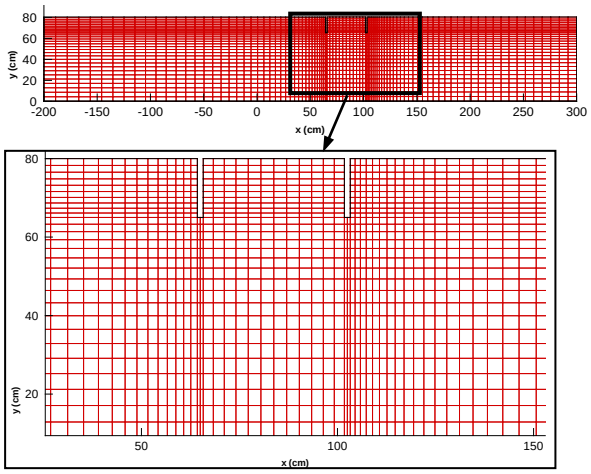

Fig.4a Grid of computed area for impermeable groins with details of groins field

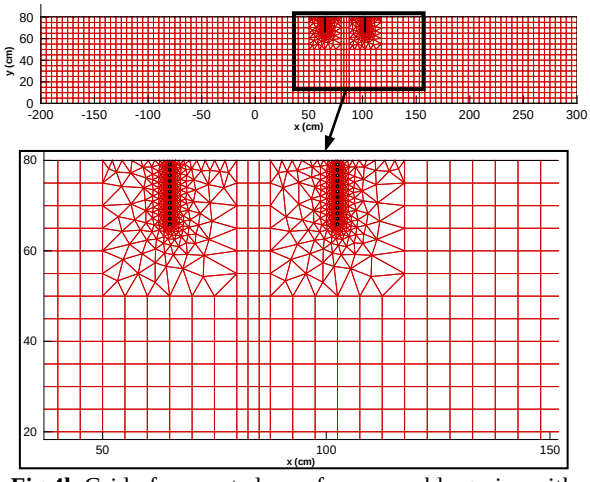

Fig.4b Grid of computed area for permeable groins with details of groins field

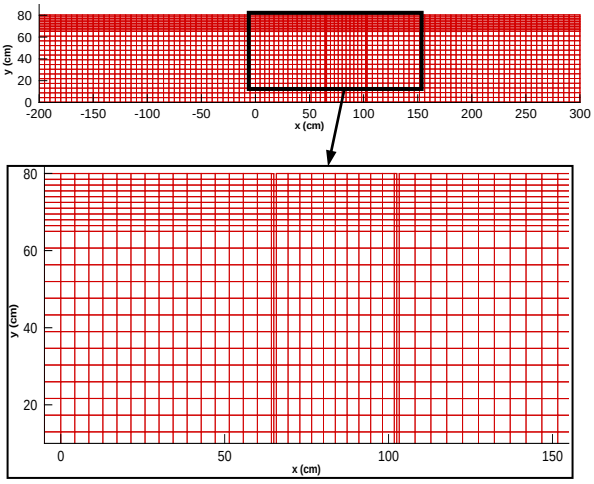

Fig.4c Grid of computed area for Bandal-like structures with details of Bandals field

In the outlet boundary at downstream, the gradient of the sediment concentration is assumed to be zero.

3. Laboratory experiments

3.1 Experimental set-up

The laboratory experiments were carried out at Ujigawa Open Laboratory, DPRI, Kyoto University, in a straight flume with 10m-long, 0.80m-wide and 0.28m-deep (0.45m-deep in the test region). The detailed sketch of the experimental set-up is shown in **Fig.5**. The channel slope was adjusted to be 1/800 m/m. The structures having a streamwise length (L) of 0.15m was embedded in a coal (powdered anthracite with d_{50}=0.835mm and ρ_s=1410kg/m^3) recess with 9.0m long, 0.80m wide and 0.10m deep (0.27m deep in the test region). The structures were fixed to the left side of the flume according to the **Fig.5**.

The coal recess is located from 2.0m downstream of the flume inlet to 1.0m upstream of flume outlet. A false floor made by wood with an elevation of 0.10m from the flume bottom and 1.0m long was fixed at the upstream end to reduce the disturbances caused in the water surface by the inlet discharge. A calibrated V-notch weir with a vernier point gauge fitted at the inlet of the flume was used to measure and control the inflow discharge. The water depth in the flume was adjusted by a steel tailgate located at the downstream end.

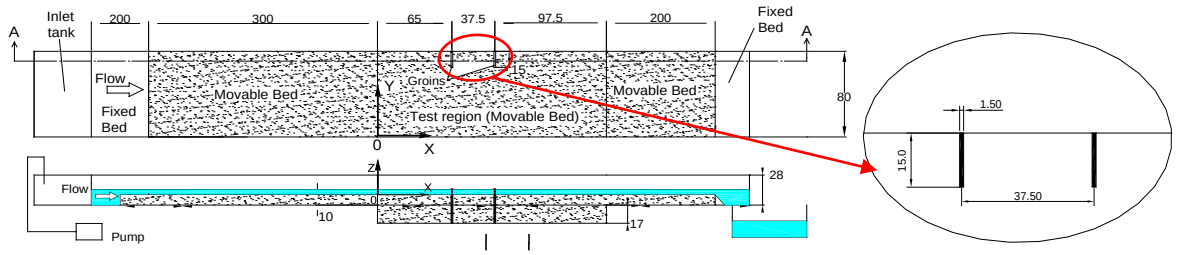

Fig.5 Experimental setup (plan-view: top; longitudinal section A-A: bottom; right side: detail of structures) (Unit:cm)

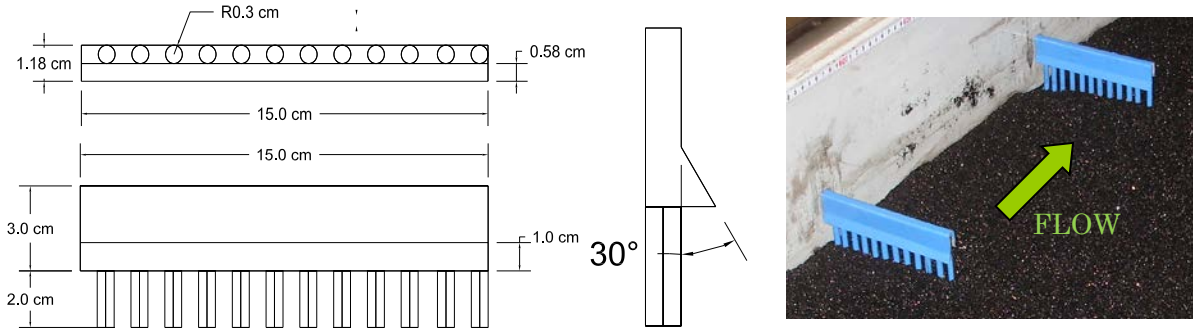

Fig.6 Detail of Bandal-like structure (top view: top-right side; front view: bottom-right side; side view: middle; position in the flume: left side)

Table 1 – Details of hydraulic conditions

Type of groin*	I	P	BS
Cases	1	2	3
Submergence	Non-submerged		
Discharge Q (l/s)	7.76		
Mean velocity u (cm/s)	24.25		
Flow depth h (cm)	4.00		
Shear velocity u_* (cm/s)	2.22		
Shear velocity ratio u_* / u_{*c}	1.91		
u_* / w_s	0.573		
Reynolds number, Re	7,406		
Froude number, Fr	0.387		

*I – Impermeable groin; P – Permeable groin; BS – Bandal-like structure

3.2 Experimental procedure

The hydraulic conditions adopted for the experiments are given in **Table 1**. Initially, the flume was slowly filled up with water by a small plastic pipe from the downstream end. Once the required water depth is reached, the correct discharge is adjusted and the experiment is started under live-bed scour condition.

The experiment was running for a period of 6 hours which is the required time to achieve the dynamic equilibrium condition accordingly to the previous test cases. After the dynamics equilibrium condition was attained the flow discharge was reduced gradually to prevent undesirable movement of the bed material and then stopped to the bed deformation measurements. In order to determine the final bed deformation contour, the remaining water was carefully drained out from the flume and the bed levels at different cross-sections were measured using a laser displacement sensor.

For the velocity measurements an instant cement powder was spread uniformly over the scoured bed to fix it. The sediment sufficiently impregnated with the cement powder was left to dry for a period of 24 h. Having dried further up to 24h, the scoured bed profile became rock hard, facilitating the flow velocity measurements. The described complex three-dimensional velocity components were measured by using electromagnetic current meters (Model: ACM250-A, Alec Electronics Co., LTD). The current meter comprised one probe with I-shape to measure the velocity in horizontal direction (plane X-Y) and another probe with L-shape to measure the velocity in the vertical direction (planes X-Z or Y-Z), connected to an analogical/digital signal converter. The probe (I or L shapes) are positioned into the water and fixed by a vernier point gauge to determine the velocity on the desired position and then connected to a

notebook through a data logger card to store the measured data. The water surface velocity measurements was realized using the PIV technique (Fujita et al., 1998) through the acquisition of flow pattern images using a video camera and PVC powder as a tracer.

The X-axis starts from the beginning of the test region (movable bed), the Y-axis from the right side wall of the flume and the Z-axis from the initial flat-bed level (**Fig.5**). The impermeable groins were made of wooden cuboids with 1.5cm thickness, while the permeable groins were made with a series of steel round sticks with a diameter equal to 0.6cm-each and designed to have a permeability of 50%. The Bandal-like structures are made using the permeable groins configuration and blocking the upper half part with a steel plate to represent the bended plate (see **Fig.6**).

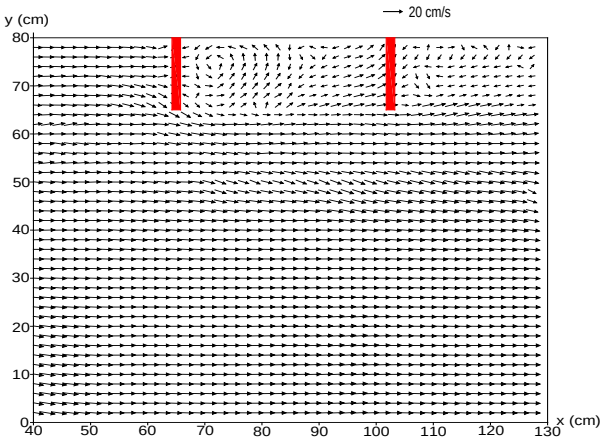

Fig.7a Flow velocity (u,v) at water surface by PIV – Impermeable groins (experiment) – Case 1

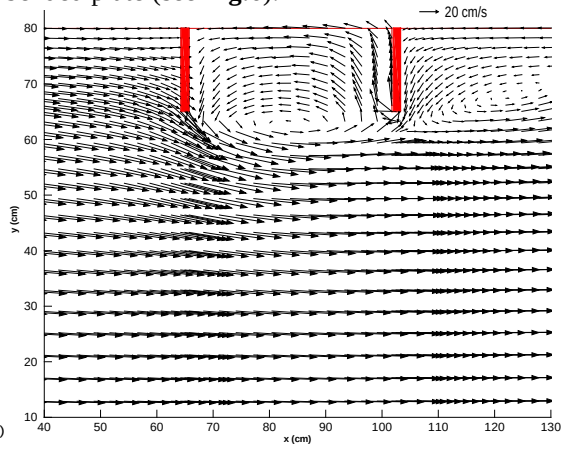

Fig.7b Flow velocity (u,v) at water surface – Impermeable groins (simulation) – Case 1

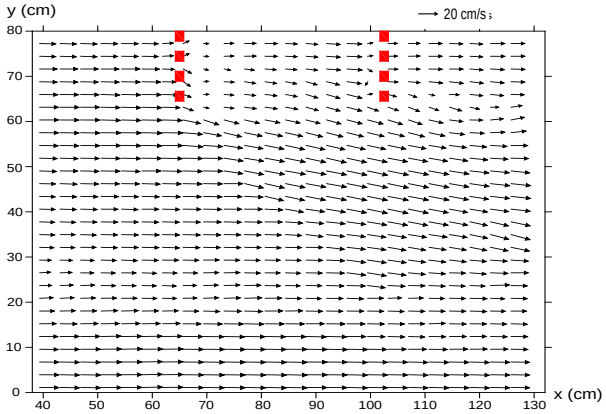

Fig.8a Flow velocity (u,v) at water surface by PIV – Permeable groins (experiment) – Case 2

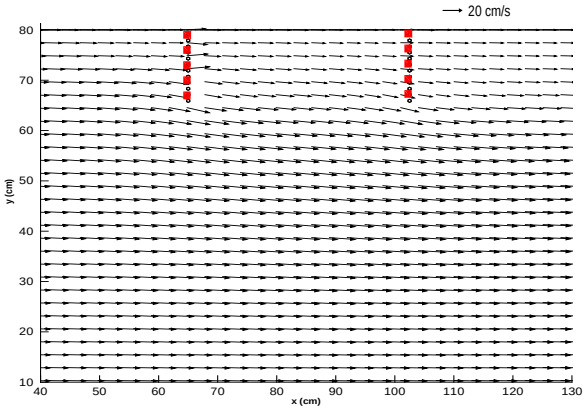

Fig.8b Flow velocity (u,v) at water surface – Permeable groins (simulation) – Case 2

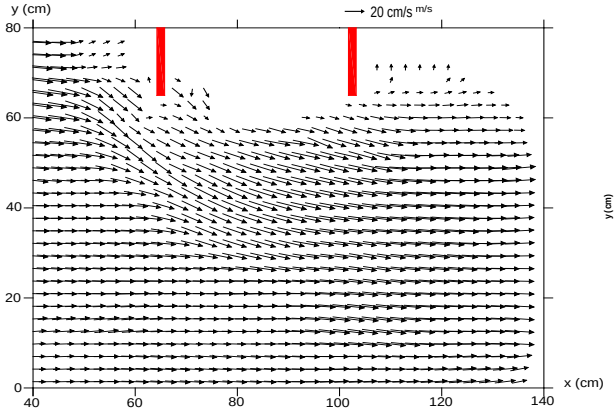

Fig.9a Flow velocity (u,v) at water surface by PIV – Bandal-like structures (experiment) – Case 3

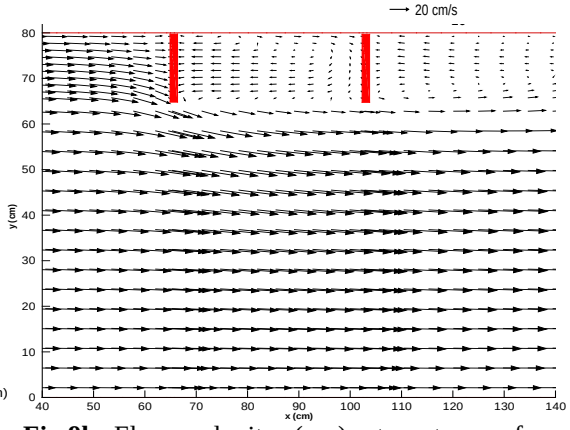

Fig.9b Flow velocity (u,v) at water surface – Bandal-like structures (simulation) – Case 3

4. Results and Discussions

4.1 Flow field around structures

The characteristics of each type of structure were analyzed through the influence on flow patterns in a straight flume. Also the applicability of numerical model was verified through the comparison between the measured flow during the laboratory experiments and the calculated flow fields. The velocity vectors at water surface around those different types of structures in horizontal plane are shown in **Figs.** 7, **8**, and **9**. The approaching flow at the upstream groin in Case 1 (**Figs.** 7**a** and **7b**) is obstructed by the impermeable groin, therefore this flow towards to the main channel direction creating a mixing zone in front of the groin head. The flow travels to downstream creating a recirculation zone in the region between the groins and also at downstream of both groins near the bank.

In comparison with the experimental measurements, the simulated results of flow field are quite similar around the structures. Due to the refinement of the mesh used in the calculations, the recirculation flow is clearly observed in the region between the two groins. The flow separation at upstream groin head is stronger in the experiments due to the tracers (PVC powder) used during the PIV measurements concentrate near the impermeable groin and it is transported as a "block" by the flow. This PVC "block" towards to the main channel in this concentrated form (**Fig.10**) giving the impression that the separation is stronger than the real.

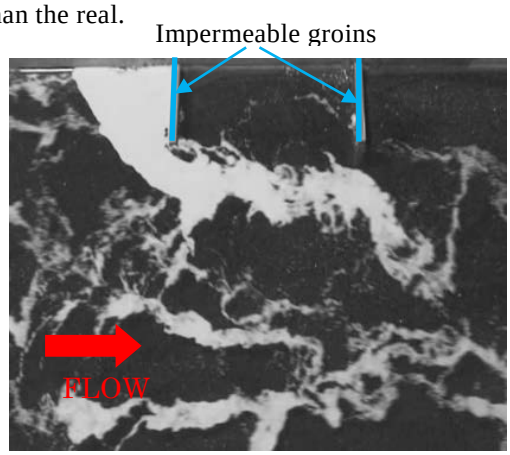

Fig.10 Visualization of flow at water surface using tracers (PVC powder) with impermeable groins.

The permeable groins (**Figs. 8a** and **8b**) show that the flow direction is not greatly changed resulting practically parallel to the channel direction. It is quite different compared to the impermeable groins case. The flow direction towards to the main channel at groins head in both experimental and simulation results, however with small intensity due to the groins permeability (**Fig.11**).

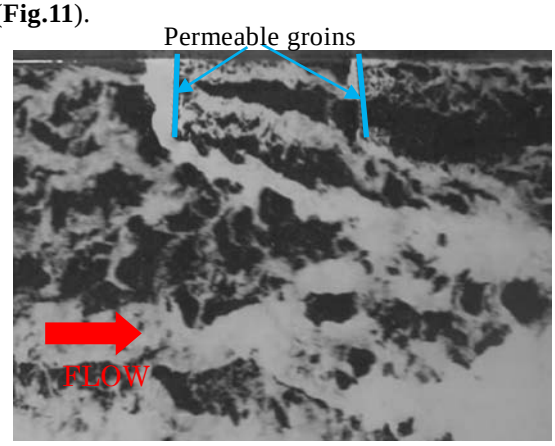

Fig.11 Visualization of flow at water surface using tracers (PVC powder) with permeable groins.

At the downstream of the upstream groin, reduction of velocity occurs near the bank and after the flow passing the downstream groin the reduction of velocity becomes more significant. This reduction is important to the riverbank protection and can contribute to the sediment deposition near the groins field.

Observing the case of Bandal-like structures, it is possible to observe differences of flow patterns especially in the area between the two structures due to the passage of flow through the lower opening of bandal (**Fig.12**).

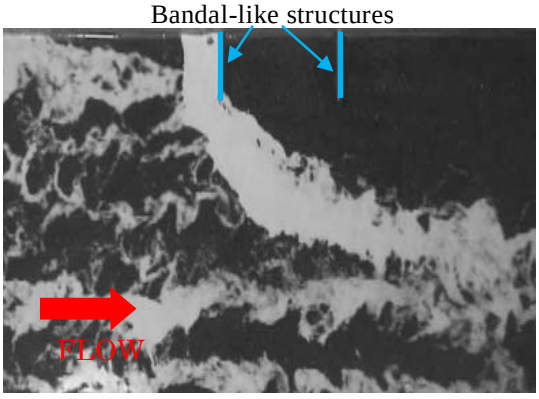

Fig.12 Visualization of flow at water surface using tracers (PVC powder) with Bandal-like structures.

In **Figs. 9a** and **9b**, it can be seen that the flow

after passing the upstream structure towards to the main channel direction, which prevents the formation of recirculation currents over there. Also a reduction of velocity magnitude occurs due to the flow separation caused by the upper half bended plate which towards the flow near the surface to the main channel direction.

To better understand the complex 3D flow structures around the structures in **Figs. 13**, **14**, **15**, and **16,** the velocity field at representative sections in vertical plane (cross-section/Y-Z plane and longitudinal-section/X-Z plane) were measured. The described sections are positioned at x=62.0cm (cross-section), just 2.25cm upstream of the upstream structure face and y=72.0cm (longitudinal-section) in the middle part of the structures (length=15.0cm).

In comparison with impermeable groins (Case 1), the Bandal-like structures (Case 3) shows similar flow patterns near the water surface due to the effect of upper half plate, i.e. the formation of downward flow caused by the blockage of flow and the vortex at upstream of Bandal. However, the flow structures at lower half portion (permeable region) show a reduction of velocity due to the presence of piles and an upward flow at downstream which causes disturbance of flow near the surface. This flow avoids the formation of recirculation flow which can be seen in the impermeable groins case.

The described downward flow in the Bandals case is weaker than the impermeable groins and it's directed to the main channel due to the effect of the upper Bandal plate. In the simulation results similar flow patterns including the vertical vortices formed near the upstream structure caused by the downward flow can be seen (**Figs. 12a** and **12b**). This feature is an important characteristic of Bandal-like structure that will be discussed in details during the analysis of bed deformation. The longitudinal-section (**Fig. 13**) shows clearly the formation of downward flow at upstream of both Bandal-like structures which induces the formation of vertical vortex at upstream of Bandals. At the downstream of each structure, the flow passing through the lower permeable part with reduced velocity show similar vertical vortex with small magnitude which avoids the formation of recirculation currents observed in impermeable groins case at the same point.

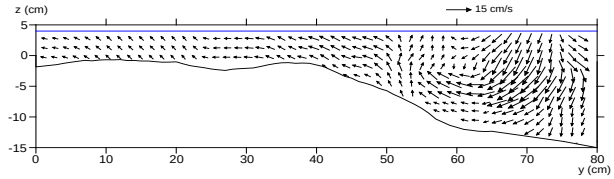

Fig.13a Transverse cross-section velocity vectors (v,w) at x=62.0cm – Case 1 (experiment)

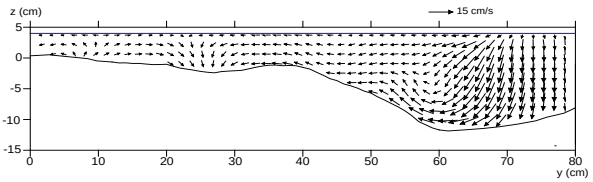

Fig.13b Transverse cross-section velocity vectors (v,w) at x=62.0cm – Case 1 (simulation)

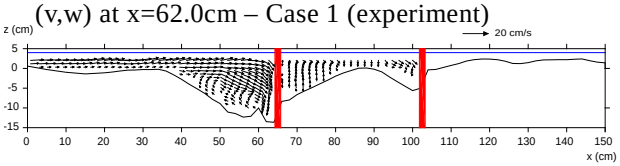

Fig.14a Longitudinal-section velocity vectors (u,w) at y=72.0cm – Case 1 (experiment)

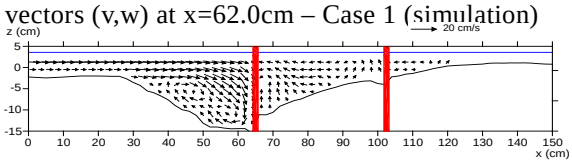

Fig.14b Longitudinal-section velocity vectors (u,w) at y=72.0cm – Case 1 (simulation)

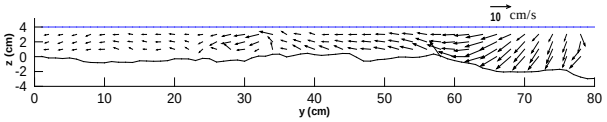

Fig.15a Transverse cross-section velocity vectors (v,w) at x=62.0cm – Case 3 (experiment)

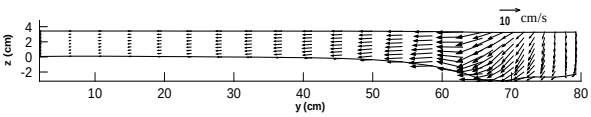

Fig.15b Transverse cross-section velocity vectors (v,w) at x=62.0cm – Case 3 (simulation)

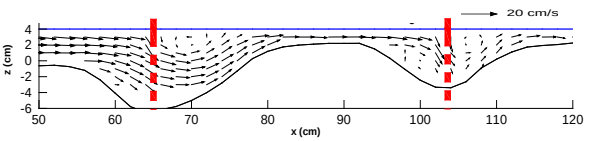

Fig.16a Longitudinal-section velocity vectors (u,w) at y=72.0cm – Case 3 (experiment)

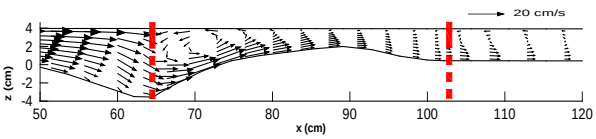

Fig.16b Longitudinal-section velocity vectors (u,w) at y=72.0cm – Case 3 (simulation)

4.2 Bed deformation

The sediment transport process is affected directly by the flow patterns around the structures described in the previous subsection. The comparisons between the experimental and simulated results of bed level contours at equilibrium condition in Cases 1, 2 and 3 are shown in details on **Figs.17**, **18** and **19**.

The widely used impermeable groins (Case 1) showed similar results verified by Rajaratnam and Nwachukwu (1983b) and Melville (1992) with huge erosion at upstream of structure, especially near the groin head. The previously described formation of downward flux due to the blockage of flow by the impermeable groin is the main reason for the deepest erosion at upstream of structure. Also, the horse shoe vortex can be seen in this region which contributes to accelerate the erosion over there. The effect of these flow structures can also be verified in the simulated results showed in **Figs. 17b** and **17c**. The area of simulated scour holes resulted smaller than that the experimental ones, however the scour depth were slight deeper.

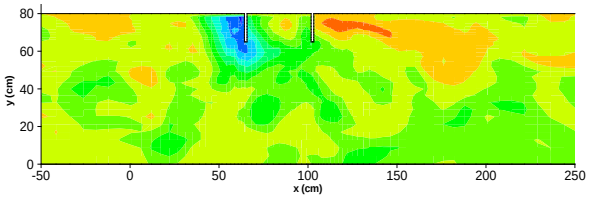

Fig.17a Bed level contour - Impermeable groins (experiment)

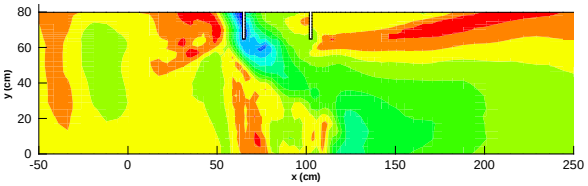

Fig.17b Bed level contour - Impermeable groins (simulation with bed-load transport)

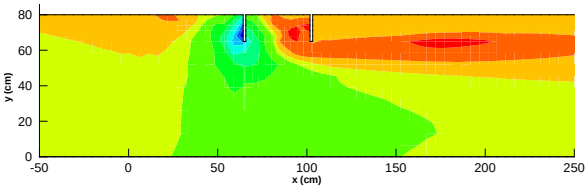

Fig.17c Bed level contour - Impermeable groins (simulation with bed-load and suspended load transport)

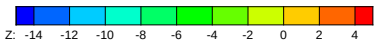

These differences are caused by the estimation of the magnitude of flow velocity and the insufficiency in linking the flow and sediment transport near the bed, especially around the structures. However, the main features of bed deformation are reproduced with acceptable results in the calculations.

In Case 3 with the Bandal-like structures, the upper bended plate towards the near surface flow with high velocities to the main channel and the flow passing through the lower part (piles) minimize the effects of the downward flux. The same effect is observed in the permeable groins (Case 2), in which the resulted erosion is very small than the other cases in both experiment and simulation (**Figs. 18a**, **18b** and **18c**) due to the weak effect to reduce the flow velocity in comparison with the Bandal-like structure case.

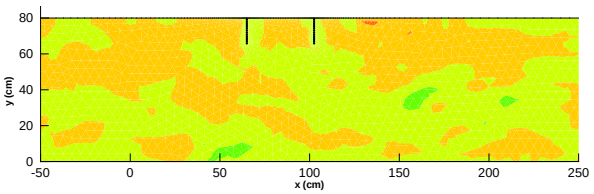

Fig.18a Bed level contour - Permeable groins (experiment)

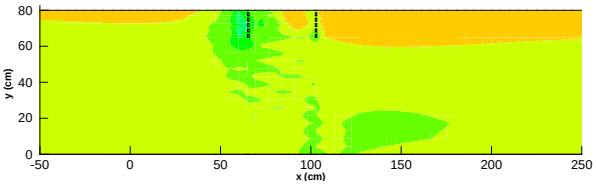

Fig.18b Bed level contour - Permeable groins (simulation with bed-load transport)

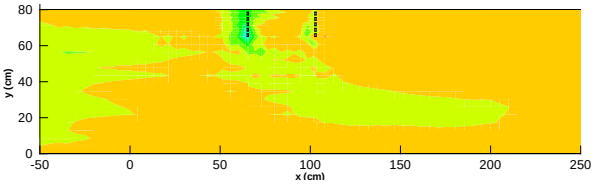

Fig.18c Bed level contour - Permeable groins (simulation with bed-load and suspended load transport)

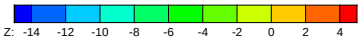

The flow separation that can be seen very clearly in Case 1 (**Fig. 7**) is responsible for the formation of recirculation currents in the region between the groins causing the erosion near the riverbank observed in **Figs. 17a**, **17b** and **17c**. At downstream of impermeable groins, the return currents with low velocities formed near the bank side cause the

deposition of sediment that is clearly verified in **Fig.17**.

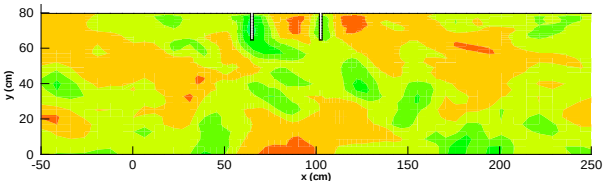

Fig.19a Bed level contour – Bandal-like structures (experiment)

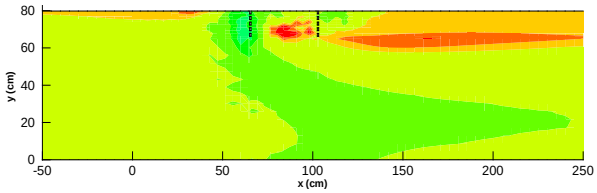

Fig.19b Bed level contour – Bandal-like structures (simulation with bed-load transport)

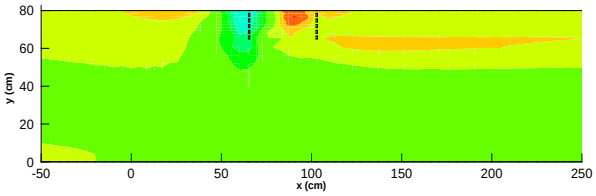

Fig.19c Bed level contour – Bandal-like structures (simulation with bed-load and suspended load transport)

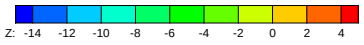

Similar flow separation occurs in the Bandal-like structures (**Figs. 19a**, **19b** and **19c**). However, due to the effect of flow passing through the lower permeable part at downstream of structure, the recirculation currents are avoided which can reduces the occurrence of erosion at river bank. Other experimental studies considering the effect of riverbank or field investigations needed to be done to verify the applicability of Bandals as a riverbank protection measure.

The deposition process around the Bandal-like structure shows promising results in comparison with other types of structures. In the region between and at downstream of structures due to the reduction of flow velocity passing through the lower opening (piles) in both structures (**Fig.16**) and the disturbances caused by the presence of piles, the deposition of the sediment transported by the flow near the bed occurs at the downstream of structure and near the bank. The inclusion of suspended sediment transport in the simulations doesn't show significant differences that the calculations with bed load transport only due to the hydraulic conditions with (u_*/w_s = 0.57) was not favorable to the occurrence of higher suspended sediment concentration. However, the applicability of Bandals to cause deposition of suspended sediment need to be verified with simulations under different hydraulic conditions.

In Case 2 with permeable groins the resulted deposition is very different because only a little reduction of flow velocity occurs and the sediment transported by the flow is carried to the downstream of channel. In this case the deposition area is distributed throughout the channel with a small concentration at downstream of groins.

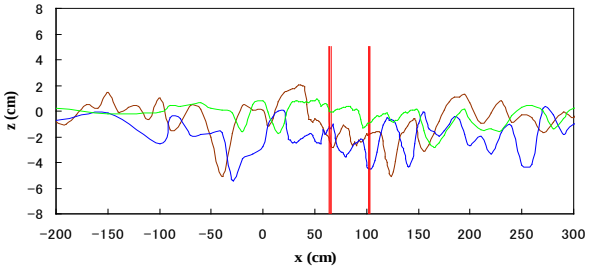

Fig.20 Longitudinal bed profile at y = 40.0cm – Case 1 (blue line), Case 2 (green line) and Case 3 (brown line) - experiment

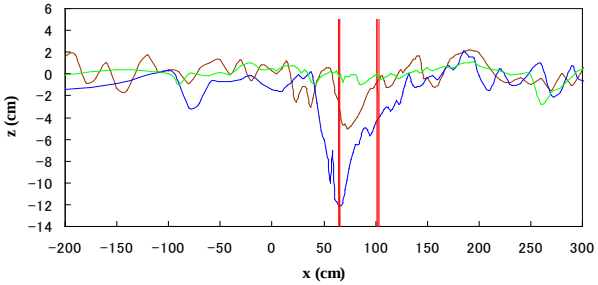

Fig.21 Longitudinal bed profile at y = 60.0cm – Case 1 (blue line), Case 2 (green line) and Case 3 (brown line) - experiment

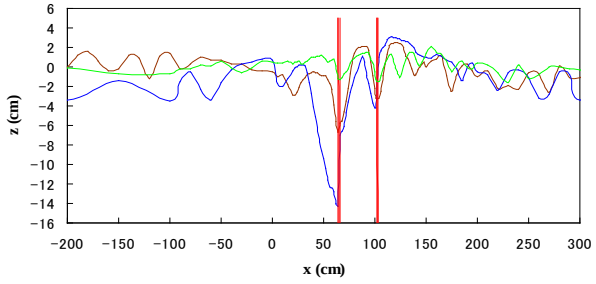

Fig.22 Longitudinal bed profile at y = 75.0cm – Case 1 (blue line), Case 2 (green line) and Case 3 (brown line) - experiment

Figs. 20, **21** and **22** show the longitudinal bed profiles at three different positions at y=40.0cm in the middle axis of flume (width = 80.0cm), y=60.0

near the structures head and y=75.0cm passing through the structures. From these figures it is possible to observe the effect of structures on bed erosion, especially near the upstream structure in Cases 1 (impermeable groins) and 3 (Bandal-likes tructures). In Case 2, the influence of structures is very weak, then the bed level variation is very small compared with other types. The local scour depth is significantly smaller around the Bandals in comparison with the conventional structures such as impermeable groins (**Fig.22**), and due to the diversion of flow towards the main channel Bandals can form a deep navigational channel (**Fig.20**). By reducing the flow velocities near the bank at downstream of structures it can ensure the protection of riverbank.

5. Conclusions

In the present study, it was investigated the characteristics of interactive action between the flow patterns and the bed variation influenced by Bandal-like structures and groins through experimental works and numerical simulations. The 3D flow field obtained from the experimental measurements under live-bed scour and non-submerged conditions was reasonable modeled. With the utilization of a sediment transport model, it can be seen that the Bandal-like structures are able to reduce the local scour depth around them in comparison with the conventional structures as impermeable groins which were observed in the experimental measurements. They also can improve the riverbank protection due to the increase on sediment deposition at downstream of the structure and consequently near the riverbank by the reduction of flow velocity which passes through the lower permeable portion of Bandals. The effect of upper plate which deviates the flow towards the main channel can be applied to the formation of deeper channel for navigation purposes and river course stabilization as well.

The numerical model is a valuable tool to deal with the river engineering problems. However, the effectiveness of this tool depends upon how well the river and structure geometry are modeled and the choice of closure model. The improvement of the modeling of a river with hydraulic structures with complex geometries can be verified through the utilization of unstructured mesh system which can represent more accurately the geometry of river morphology. The choice of the turbulence model has a significant influence on the flow details. In the numerical model used in this study, the standard k-ε model was utilized with reasonable representation of separation zones and the flow regions having the spiral motion. Improvement of the model using a non-linear k-ε model are expected to better represent with good accuracy the described formation of vortex in the disturbed regions. Another problem that limits the application of 3D morphodynamic model is the long CPU time needed for the calculations.

Further investigations of the applicability of Bandal-like structures through the laboratory experiments, numerical simulations and also field applications are expected to prove the effectiveness of this structure in different conditions.

References

Ashida, K. and Michiue, M. (1972): Studies on bed load transportation for nonuniform sediment and river bed variation, Disaster Prevention Research Institute Annuals, Kyoto University, No. 14B, pp. 259-273 (in Japanese).

Carling, P.A., Kohmann, F., and Golz, E. (1996): River hydraulics, sediment transport and training works: their ecological relevance to European rivers, Archiv. Hydrobiol. Suppl., Vol. 113, No. 10, pp 129-146.

Copeland, R. R. (1983): Bank protection techniques using spur dikes, Hydraulics Laboratory, U.S. Army Corps of Engineers, Waterways Experiment Station, Vicksburg, Mississippi.

Dey, S., and Barbhuiya, A. K. (2006): Velocity and turbulence in a scour hole at a vertical-wall abutment, Flow Measurements and Instrumentation, Vol. 17, pp. 13-21.

Fujita, I., Muste, M., and Kruger, A. (1998): Large scale particle image velocimetry fro flow analysis in hydraulic engineering applications, Journal of Hydraulic Research, vol. 36, No. 3, pp. 397-414.

Garde, R. J., Subramanya, K. and Nambudripad, K. D. (1961): Study of scour around spur-dikes, Journal of Hydraulic Division, ASCE, Vol. 87, No.

6, pp. 23-38.

Gill, M.A. (1972): Erosion of sands beds around spur dikes, Journal of Hydraulic Division, ASCE, Vol. 98, No. 9, pp. 1587-1602.

Jameson, A., Schmidt, W., and Turkel, E. (1981): Numerical solution of the Euler equations by finite volume methods using Runge-Kutta time stepping schemes, Technical Report AIAA-81-1259, AIAA 14th Fluid and Plasma Dynamics Conference, Palo Alto, C. A.

Kothyari, U. C., and Ranga Raju, K. J. (2001): Scour around spur dikes and bridge abutments, Journal of Hydraulic Research, Vol. 39, No. 4, pp. 367-374.

Kuhnle, R. A., Alonso, C. V., and Shields, F. D. (1999): Geometry of scour holes associated with 90o spur dikes, Journal of Hydraulic Engineering, ASCE, Vol. 125, No. 9, pp. 972-978.

Launder, B .E., and Spalding, D. B. (1973): The numerical computation of turbulent flows, Computer Methods in Applied Mechanics and Engineering, Vol. 3, pp. 269-289.

Melville, B. W., and Coleman, S. E. (2000): Bridge Scour, Water Resources Publications, Highlands Ranch, Colorado.

Mioduszewski, T., Maeno, S., and Uema, Y. (2003): Influence of the Spur Dike Permeability on Flow and Scouring during a Surge Pass, International Conference on Estuaries and Coasts, Hangzhou, China, pp. 380-388.

Nagata, N., Hosoda, T., Nakato, T., and Muramoto, Y. (2005): Three-dimensional numerical model for flow and bed deformation around river hydraulics structures, Journal of Hydraulic Engineering, ASCE, Vol. 131, No. 12, pp. 1074-1087.

Nasrollahi, A., Ghodsian, M., and Salehi Neyshabouri, S. A. A. (2008): Local scour at permeable spur dikes, Journal of Applied Sciences, Vol. 8, No. 19, pp. 3398-3406.

Onda, S., Hosoda, T., Kimura, I., and Iwata, M. (2007): Numerical simulation on local scouring around a spur dyke using equilibrium and non-equilibrium sediment transport models, Annual Journal of Hydraulic Engineering, JSCE, Vol. 51, pp. 943-948.

Patankar, S. V. (1980): Numerical Heat Transfer and Fluid Flow, Hemisphere, New York.

Rahman, M. M., Nakagawa, H., Khaleduzzaman, A. T. M., Ishigaki, T., and Muto, Y. (2004): On the formation of stable river course, Annuals of Disaster Prevention Research Institute, Kyoto University, No. 47B, pp. 601-616.

Rahman, M. M., Nakagawa, H., Ito, N., Haque, A., Islam, T., Rahman, M. R., and Hoque, M. M. (2006): Prediction of Local Scour Depth around Bandal-like Structures, Annual Journal of Hydraulic Engineering, JSCE, Vol. 50, pp. 163-168.

Rajaratnam, N, and Nwachukwu, B. A. (1983): Flow near groyne-like structures, Journal of Hydraulic Engineering, ASCE, Vol. 109, No. 3, pp. 463-480.

Rodi, W. (1980): Turbulence models and their application in hydraulics – a state of art review, University of Karlsruhe, Germany.

Rouse, H. (1937): Modern conceptions of the mechanics of fluid turbulence, ASCE Transactions, Vol. 102, pp. 436-505.

Sharmin, R., Rahman, M. M., Martin, A., Haque, E., Hossain, I., and Razzak, A. (2007): Effectiveness of Bandalling and dredging for the maintenance of navigation channel in the Jamuna River, Int. Conf. on Water & Flood Management, March 12-14, Dhaka, Bangladesh, pp. 125-133.

Shields, F. D., Jr., Copeland, R. R., Klingeman, P. C., Doyle, M. W., and Simon, A. (2003): Design for stream restoration, Journal of Hydraulic Engineering, Vol. 129, No. 8, pp. 575-584.

Shimizu, Y., Yamaguchi, H., Itakura, T. (1990): Three-dimensional computational of flow and bed deformation, Journal of Hydraulic Engineering, ASCE, Vol. 116, No. 9.

Sleijpen, G L. G., and Fokkema, D. R. (1993): BiCGSTAB(*l*) for linear equations involving unsymmetrical matrices with complex spectrum, Electronic Transactions on Numerical Analysis, Ken State University, Vol. 1, pp. 11-32.

Uijttewaal, W. S. J. (2005): Effects of groin layout on the flow in groin fields: laboratory experimental, Journal Hydraulic Engineering, ASCE, Vol. 131, No. 9, pp. 782-791.

Van Rijn, L. C. (1987): Mathematical modeling of morphological processes in the case of suspended sediment transport, Delft Hydra. Communication No. 382, Delft, the Netherlands.

Versteeg, H. K., and Malalasekera, W. (1995): An

Introduction to Computational Fluid Dynamics, Longman: Harlow, pp. 103-155, U. K.

Wang, S. S. Y., and Adeff, S. E. (1986): Three-dimensional modeling of river sedimentation processes, Proc., 3rd International Symposium on River Sedimentation, The University of Mississippi, Missouri, pp. 1594-1601.

Wang, S. Y., and Jia, Y. (1995): Computational modeling and hydro science research, Advances in Hydro-Science and Engineering, in Proceedings of 2nd International Conference on Hydro-Science and Engineering, Beijing, Tsinghua University Press, pp. 2147-2157.

Wu, W., Rodi, W., and Wenka, T. (2000): 3D numerical modeling of flow and sediment transport in open channels, Journal of Hydraulic Engineering, Vol. 126, No. 1, pp. 4-15.

Zhang, H., Nakagawa, H., Muto, Y., Baba, Y. and Ishigaki, T. (2006): Numerical simulation of flow and local scour around hydraulic structures, River flow 2006, pp. 1683-1693.

Zhang, H., and Nakagawa, H. (2009): Characteristics of Local Flow and Bed Deformation at Impermeable and Permeable Spur Dykes, Annual Journal of Hydraulic Engineering, JSCE, Vol. 53, pp. 145-150.

バンダル型水制の河床変動に関する研究

中川一・Hiroshi TERAGUCHI・川池健司・馬場康之・張浩

要　旨

本研究は，バンダル型水制周辺の流れがもたらす河床変化に着目した．バンダル型水制はインド亜大陸で古くから用いられており，バングラデシュを流れるジョナム川のような沖積河川では，河岸浸食の防止，航路の維持を目的として設置されている．しかし，透過型・不透過型水制のような従来から用いられている治水構造物の代用として，バンダル型水制が真に有効であるかを検証した研究や現地調査は少ない．そこで，バンダル型水制が河川形態にもたらす影響を明らかにするために，バンダル型水制による複雑な流れや流砂メカニズムについて検討を行った．片側に２基の水制を設置した直線水路を用いて，動的洗掘状態の移動床実験を行い，水制周辺の河床位の計測と洗掘河床上の流れ場の計測を行った．数値解析モデルでは非構造メッシュを用いており，各水制タイプについて流れと河床変動の計算を行った．これらの実験および計算結果を分析し，バンダル型水制が従来の水制と比べて周辺の局所洗掘を低減し，水制背後への土砂堆積を促すのに有効であることを示した．

キーワード：バンダル型水制，動的洗掘状態，３次元モデル，非越流